


Changwoo LEE,¹ Yonghui PARK ²

Optimization of gear teeth in the wind turbine drive train with gear contact's uncertainty using the reliability-based design optimization

Received 11 January 2022, Revised 25 May 2022, Accepted 5 July 2022, Published online 16 November 2022

Keywords: wind turbine, drive train, gear, structural analysis, dynamics, Fourier transform, reliability based design optimization

Although gear teeth give lots of advantages, there is a high possibility of failure in gear teeth in each gear stage in the drive train system. In this research, the authors developed proper gear teeth using the basic theorem of gear failure and reliability-based design optimization. A design variable characterized by a probability distribution was applied to the static stress analysis model and the dynamics analysis model to determine an objective function and constraint equations and to solve the reliability-based design optimization. For the optimization, the authors simulated the torsional drive train system which includes rotational coordinates. First, the authors established a static stress analysis model which gives information about endurance limit and bending strength. By expressing gear mesh stiffness in terms of the Fourier series, the equations of motion including the gear mesh models and kinematical relations in the drive train system were acquired in the form of the Lagrange equations and constraint equations. For the numerical analysis, the Newmark Beta method was used to get dynamic responses including gear mesh contact forces. From the results such as the gear mesh contact force, the authors calculated the probability of failure, arranged each probability and gear teeth, and proposed a reasonable and economic design of gear teeth.

✉ Yonghui Park, e-mail: yhpark@yuhan.ac.kr

¹Pohang Institute of Metal Industry Advancement, Pohang, Republic of Korea

²Department of Mechanical Engineering, Yuhan University, Bucheon, Republic of Korea. ORCID: 0000-0001-6716-6935



© 2022. The Author(s). This is an open-access article distributed under the terms of the Creative Commons Attribution (CC-BY 4.0, <https://creativecommons.org/licenses/by/4.0/>), which permits use, distribution, and reproduction in any medium, provided that the author and source are cited.

1. Introduction

In the energy crisis, many countries have carried out research on alternative energy sources. A wind turbine is the most popular alternative in the energy industry and intensive research is being done in this field [1–3]. Recently, the development of lighter and more stable structures concentrates especially on the blades. However, the most important characteristic of the wind turbine is rotation. From the rotor, the drive train delivers torque to the generator. It would be important to find a new, lighter drive structure. But, the dynamic characteristics of the drive train should be considered first.

In this research, the authors considered a torsional drive train that has rotational coordinates. In the previous research, the torsional model which had a gear mesh [4], and a more detailed 2-dimensional model [5] were investigated with parametric analysis. The common concept of the two researches is analyzing the vibrational results from the gear mesh. If there is an external torque, the gear contact will occur repeatedly. So, the main characteristic of rotation can be determined by the contact force. The mentioned researches [4, 5] showed the contact force in the time and frequency domain. The gear mesh makes rotational motion and simultaneously its angular velocity changes. Gears have been applied in lots of industries including automobile and aircraft, etc. Although it gives more advantages than disadvantages, there is a risk caused by the gears, especially the gear teeth. If there are cracks or wear in the gear teeth, one cannot identify the defects clearly, and finally cannot prevent the face fatigue failure. In this view, many researchers have tried to find out the best design suitable for the gears.

This research shows a proper gear teeth design by calculating the gear mesh contact force. Especially, the authors assumed that there are uncertainties in manufacturing. These uncertainties make the material non-isotropic which causes defects and damages and creates problems with strengths. To deal with these problems, some authors use mechanical components which have non-perfect properties. Unfortunately, these problems cannot be handled and solved by the authors of the present study. Our task is to find proper reliability which satisfies system safety and economic efficiency standards. After setting the number of gears, the design variable and calculating the gear teeth bending stress and endurance limit, constraint and the gear mesh model uncertainty, the authors analyzed the gear mesh model using the torsional drive train model and reliability-based design optimization. The authors compared the reliability of the gear contact force and ratio taking into account several candidates for the gear teeth, in order to find out the optimized gear teeth. Gear teeth bending stress and endurance limit were designed based on the Lewis theorem [6]. Also, the gear mesh stiffness models were defined by the Fourier series. All the analyses were computed by the Newmark method, which is a kind of numerical integration method. It shows gear teeth information including reliability and the number of teeth.

2. Mathematical model

2.1. Gear mesh model

Generally, the spring connected between two components has a constant stiffness and exerts a reaction force relative to the displacement of the two contact points. In the gear mesh, the reaction of the contact surface between a pinion and a gear can be represented by the spring. However, in the case of gears, the periodic change in a component must be represented. Gear mesh stiffness is determined by the angle of attack and contact ratios [4, 7]. Considering this fact, the authors defined the gear mesh stiffness using angular velocity and contact ratio of the gear. In this research, the authors used the rotor's angular velocity of 10 rad/s as the standard. So, the average angular velocities in the planetary stage and the parallel stages were defined by Equations (1), (2), and (3), respectively. Then, the authors established gear mesh stiffness by using the Fourier series including these angular velocities. ω_C , ω_{g1} , and ω_{g3} are the angular velocities of the carrier, gear 1 and gear 3, respectively. N_r , N_{g1} and N_{g3} are the number of teeth of the ring gear, gear 1 and gear 3, respectively. $\omega_M^{(p)}$, $\omega_M^{(g12)}$ and $\omega_M^{(g34)}$ are the gear mesh frequency in the planetary stage and in the parallel stages, respectively.

$$\omega_M^{(P)} = \omega_C N_r, \quad (1)$$

$$\omega_M^{(g12)} = \omega_{g1} N_{g1}, \quad (2)$$

$$\omega_M^{(g34)} = \omega_{g3} N_{g3}, \quad (3)$$

For instance, Equations (4) and (5) represent the gear mesh stiffness of the planetary gear stage, and Fig. 1 is the plot of the gear mesh stiffness of the planetary gear stage. γ_{sp} , γ_{rs} , and γ_{rp} are phase difference factors which represent the variable gear mesh between the sun gear, the planet gear and the ring gear, C_{rp} and C_{sp} are contact ratios for the ring-planet and the sun-planet gear pairs.

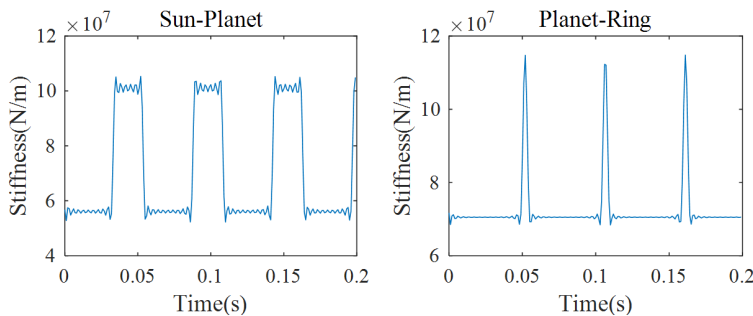


Fig. 1. Gear mesh stiffness

$$k_{sp}(t) = k_{sp} + \frac{k_{sp}}{C_{sp}} \sum_{l=0}^{\infty} \left(a_{sp}^{(l)} \sin(\omega_M^{(p)} t) + b_{sp}^{(l)} \cos(\omega_M^{(p)} t) \right), \quad (4)$$

$$k_{rp}(t) = k_{rp} + \frac{k_{rp}}{C_{rp}} \sum_{l=0}^{\infty} \left(a_{rp}^{(l)} \sin(\omega_M^{(p)} t) + b_{rp}^{(l)} \cos(\omega_M^{(p)} t) \right), \quad (5)$$

where

$$a_{sp}^{(l)} = -\frac{2}{l\pi} \sin [l\pi(C_{sp} - 2\gamma_{sp})] \sin(l\pi C_{sp}),$$

$$b_{sp}^{(l)} = -\frac{2}{l\pi} \cos [l\pi(C_{sp} - 2\gamma_{sp})] \sin(l\pi C_{sp}),$$

$$a_{rp}^{(l)} = -\frac{2}{l\pi} \sin [l\pi(C_{sp} - 2\gamma_{sp} - 2\gamma_{rs})] \sin(l\pi C_{rp}),$$

$$b_{rp}^{(l)} = -\frac{2}{l\pi} \cos [l\pi(C_{rp} - 2\gamma_{rp} - 2\gamma_{rs})] \sin(l\pi C_{rp}).$$

2.2. Equations of motion using torsional dynamics

As presented in Fig. 2, the applied wind turbine drive train model includes the rotor, the carrier, the planetary stage, the parallel stages and the generator [8–15]. Each component was considered a rigid body. There are three main shafts between the rotor and the carrier, the sun and the gear 1, and the gear 3 and

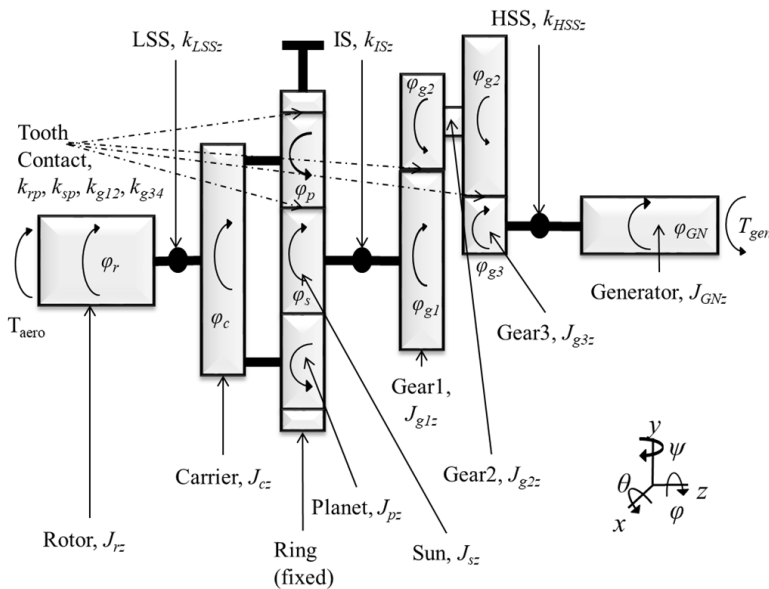


Fig. 2. Diagram of the drive train system

the generator. We defined these connectors as torsional springs that drive powers among relative components. Design variables including the moment of inertia and mass of each component and stiffness of the connector were taken from the previous research [4]. By deriving equations of motion from Lagrange's equation, we can express the equations of motion with mass, damping, and stiffness matrix with respect to the generalized coordinates. When the mass, damping, and stiffness matrices are defined, it is necessary to determine each moment of inertia, mass, and relative displacement of two points that are connected by a spring.

In a gear, rotation is changing to translation. It is illogical if the authors think that two revolving bodies meet and give torque to each other. But, the authors can find translational relationships through the point concepts. In other words, two points will meet and fall apart by exerting a contact force. Through this contact force, the gear will rotate by a torque. Based on general information about the drive train, the authors need to derive the equation of motion with the gear mesh model for calculating the state variables such as angular displacement and angular velocity for determining the gear mesh contact force and for making the comparison with standards, and for optimization of the gear. They need to find out whether the gear mesh, including its uncertainty, is acceptable or not.

To derive the equation of motion, the Lagrange equation method was used to calculate the state variables [16, 17]. Among the system properties, the gear mesh stiffness will change every time. So, the authors represent these changes in the stiffness matrix. Regarding relative displacement, the authors showed an example of rotational motions about the z -axis and translation motions about the x - y plane in equation (6)–(12). Equation (6) is the relative torsional displacement of the low-speed shaft, equations (7)–(8) are the relative gear mesh displacements of the sun-planet and the ring-planet gear mesh, and equation (9) is the relative torsional displacement of the internal shaft, equations (10)–(11) are the relative gear mesh displacements of the gear 1-gear 2 and the gear 2-gear 3 gear mesh, and equation (12) is the relative torsional displacement of the high-speed shaft. These were used to define the total potential energy which is the elastic energy stored in the springs which represent the shaft and the gear in Fig. 2.

$$\phi_{LSS} = \phi_{\text{rotor}} - \phi_{\text{carrier}}, \quad (6)$$

$$\delta_{\text{planet-sun}} = -r_{\text{carrier}}\phi_{\text{carrier}} + r_{\text{planet}}\phi_{\text{planet}} + r_{\text{sun}}\phi_{\text{sun}}, \quad (7)$$

$$\delta_{\text{planet-ring}} = r_{\text{carrier}}\phi_{\text{carrier}} + r_{\text{planet}}\phi_{\text{planet}}, \quad (8)$$

$$\phi_{IS} = \phi_{\text{sun}} - \phi_{G1}, \quad (9)$$

$$\delta_{G1-G2} = r_{G1}\phi_{G1} + r_{G2}\phi_{G2}, \quad (10)$$

$$\delta_{G2-G3} = r_{G2}\phi_{G2} + r_{G3}\phi_{G3}, \quad (11)$$

$$\phi_{HSS} = \phi_{G3} - \phi_{GN}. \quad (12)$$

Equations (13) and (14) are the total kinetic energy of the total rotors and the potential energy among the shafts and gear meshes in the drive train system.

$$T = \frac{1}{2}J_{r_z} (\dot{\phi}_r)^2 + \frac{1}{2}J_{c_z} (\dot{\phi}_c)^2 + \frac{3}{2}m_p (r_c \dot{\phi}_c)^2 + \frac{3}{2}J_{p_z} (\dot{\phi}_p)^2 + \frac{1}{2}J_{s_z} (\dot{\phi}_s)^2 + \frac{1}{2}J_{g1_z} (\dot{\phi}_{g1})^2 + \frac{1}{2}J_{g2_z} (\dot{\phi}_{g2})^2 + \frac{1}{2}J_{g3_z} (\dot{\phi}_{g3})^2 + \frac{1}{2}J_{GN_z} (\dot{\phi}_{GN})^2, \quad (13)$$

$$V = \frac{1}{2}k_{LSS_z} (\dot{\phi}_{LSS})^2 + \frac{1}{2}k_{IS_z} (\dot{\phi}_{IS})^2 + \frac{1}{2}k_{HSS_z} (\dot{\phi}_{HSS})^2 + \frac{3}{2}k_{rp} (\delta_{\text{planet-ring}})^2 + \frac{3}{2}k_{sp} (\delta_{\text{planet-sun}})^2 + \frac{1}{2}k_{g12} (\delta_{G1-G2})^2 + \frac{1}{2}k_{g34} (\delta_{G2-G3})^2. \quad (14)$$

Using the kinetic and potential energy terms, the authors derived the Lagrange equation and the equations of motion according to the vector of the generalized coordinates. Equations (15)–(17) illustrate the process of determining the equation of motion. Equation (16) in conjunction with Equations (14)–(15) yields coupled ordinary differential equations in the conventional form, and the equations of motion in a matrix form are given as equation (17). Q is the vector of the generalized forces which include gravity and the non-linear forces that cannot be defined as a matrix, in such a way as the mass matrix $[J]$, the damping matrix $[C]$, and the stiffness matrix $[K]$. This vector will be applied to the right side of Equations (16) and (17). Finally, we can get dynamic results from the equations of motion (Eq. (17)) by using numerical integrations such as the Newmark's method.

$$L = T - V. \quad (15)$$

where T is the kinetic energy, and V is potential energy

$$\frac{d}{dt} \left(\frac{\delta L}{\delta \dot{q}_j} \right) - \frac{\delta L}{\delta q_j} = \vec{Q}_j, \quad j = 1, 2, 3, \dots, 8. \quad (16)$$

Here $\vec{Q}_j = \vec{Q}_g(t) + \vec{Q}_{\text{ext}}(t)$

$$[J] \ddot{\vec{\phi}} + [C] \dot{\vec{\phi}} + [K] \vec{\phi} = \vec{Q}_j. \quad (17)$$

2.3. Simulation condition

For the numerical method, the authors used the Newmark's beta method [18, 19]. Table 1 [5] shows basic information about the drive train. Some information is not provided, such as the number of the gear teeth, but the authors could use fundamental theorems of the mechanical components, such as those of gear design, to specify the design details based on the available information, such as the gear contact ratios. With respect to simulation conditions, the authors assumed that the aerodynamic torque was $T_{\text{aero}} = 15\,000$ Nm, and the electromagnetic torque was -30% of the aerodynamic torque, which corresponded to 30% of wind turbine efficiency. The rotor was exited with an angular velocity of 10 rad/s.

Table 1. Data for the drivetrain configuration presented in this work

J_{rz}	inertia of the rotor ($\text{kg}\cdot\text{m}^2$)	$4.18\cdot 10^6$
J_{cz}	inertia of the carrier ($\text{kg}\cdot\text{m}^2$)	57.72
J_{pz}	inertia of the planet ($\text{kg}\cdot\text{m}^2$)	1.12
J_{sz}	inertia of the sun ($\text{kg}\cdot\text{m}^2$)	0.86
J_{g1z}	inertia of the gear 1 ($\text{kg}\cdot\text{m}^2$)	14.32
J_{g2z}	inertia of the gear 2 ($\text{kg}\cdot\text{m}^2$)	1.62
J_{g3z}	inertia of the gear 3 ($\text{kg}\cdot\text{m}^2$)	0.20
J_{GNz}	inertia of the generator ($\text{kg}\cdot\text{m}^2$)	93.22
k_{LSSz}	torsional stiffness about z-axis of the LSS (Nm/rad)	$7.19\cdot 10^7$
k_{ISz}	torsional stiffness about z-axis stiffness of the IS (Nm/rad)	$1.40\cdot 10^7$
k_{HSSz}	torsional stiffness about z-axis of the HSS (Nm/rad)	$0.15\cdot 10^7$
k_{rp}, k_{sp}	stiffness of the engaging tooth pairs in the low speed planetary gear stage (N/m)	$0.73\cdot 10^8$
k_{g12}	stiffness of the engaging tooth pairs in the 1st high-speed parallel gear stage (N/m)	$2.02\cdot 10^9$
k_{g34}	stiffness of the engaging tooth pairs in the 2nd high-speed parallel gear stage (N/m)	$0.11\cdot 10^8$
C_{rp}	contact ratio of ring-planet	1.9342
C_{sp}	contact ratio of sun-planet	1.6242
C_{g12}	contact ratio of gear 1 and 2-1	1.6616
C_{g34}	contact ratio of gear 2-1 and 3	1.5984
r_c	radius of carrier (m)	0.270
r_p	radius of planet (m)	0.160
r_s	radius of sun (m)	0.110
r_{g1}	radius of gear 1 (m)	0.290
r_{g2_1}	radius of gear 2_1 (m)	0.095
r_{g2_2}	radius of gear 2_2 (m)	0.185
r_{g3}	radius of gear 3 (m)	0.080
α	pressure angle ($^\circ$)	0.020
Gear ratio		34.654

3. Optimization

3.1. Reliability-based design optimization

Reliability is the figure of merit to judge product function [20–25]. In reliability-based design optimization, reliability means that products satisfy functionality by probability. If there is a failure from a non-isotropic material or manufacturing error, we should represent product reliability as a quantitative value. A good way is to represent reliability as a random variable. Equation (18) shows the constraint

equation where the limit state function is represented by a random variable [26]. R and S are structural resistance and structural load effect, respectively. The authors specified the sun-planet, the ring-planet, the gear 1-gear 2, and the gear 2-gear 3 contact ratios as the random variables X_1 – X_4 , respectively, according to the number of gear teeth and their uncertainty.

$$G(X_i) = G(X_1, X_2, X_3, \dots, X_i) = R(X_1, X_2, X_3, \dots, X_i) - S(X_1, X_2, X_3, \dots, X_i). \quad (18)$$

From equation (18), failure and safe region can be defined as $G(X_i) \leq 0$ and $G(X_i) > 0$, respectively. Equation (19) is the joint-probability density function that defines the probability of failure.

$$P_f = P[G(X_i) \leq 0] = \int_{G(X_i) \leq 0} f_x(X_i) dX. \quad (19)$$

The probability of safety is the opposite to the probability of failure. In this research, the authors computed reliability to make an optimized gear teeth model with gradient algorithms used in the determination of the random variables.

According to design optimization, the authors defined general terms for acquiring optimized solutions. All of the system properties of the drive train except the gear mesh were taken from the research by Todorov et al. [5]. Although the gear teeth are different, the performances including the gear ratio should be equal when these properties are used. In other words, the obtained gear relationships should be the same. According to this fact, the authors can classify the terms as design variables, objective functions, and constraints. First, the design variables are the number of gear teeth. Basic information about the gear including the pitch diameter, the gear ratio, and the contact ratio should be identical to perform the same angular motion. But, the number of gear teeth maintaining the same gear ratio can be different. As referred before, our task is to determine the proper number of gear teeth that satisfy safety standards. To evaluate safety standards, we assumed uncertainty of manufacturing error by adding the contact ratio's probability. If there are errors in the process, every contact ratio will show the same errors caused by the machine tool. So, the authors inputted different gear mesh models that included uncertainty in the contact ratio with errors having the same pattern of normal distribution.

Secondly, the objective function is a certain function of gear mesh contact forces' probability. The gear mesh contact force can be calculated by multiplying the gear mesh stiffness from equations (1)–(5) in Section 2.1 and the relative displacement from equations (7), (8), (10) and (11) in Section 2.2. The authors obtained probability results arranged according to the number of gear teeth. In another problems, most of researchers tried to find out a proper value which coincides with the minimum objective function. However, the authors developed an algorithm that provides high reliability according to the standards and chose the minimum number of gear teeth.

Finally, the constraints are the other properties except for the design variables that include the gear teeth bending strength criterion in Section 3.2 [6]. As have been mentioned before, basic design variables including the inertia of the rotor were listed in Table 1 except for the applied variables such as the contact ratio. In other words, if design variables are defined, other properties are defined by kinematical relation equations. For instance, Equations (20) and (21) are the gear ratio and gear relationship of planetary gear stages.

$$\text{Ratio} = \frac{R + S}{S}, \quad (20)$$

$$R = 2 \times P + S. \quad (21)$$

From these relationships, the authors can define the sun and planet gear teeth from the ring gear. This is one example of constraints. In the work by Todorov et al. [5] regarding Table 1, the authors just showed gear contact ratios instead of the number of gear teeth. The authors could determine the number of gear teeth by substituting the determined number of gear teeth in Equations (20) and (21). By the same procedure, the authors could define all the design variables including gears 1, 2, and 3.

Consequently, the authors obtained the probability and the number of gear teeth in every simulation. Some of them satisfied safety standards, the others didn't. Above the specific number of gear teeth, all greater numbers of the gear teeth give high reliability. Because of safety, all of them satisfy standards. However, the goal of engineering design is to generate economic profits. Using small amounts of materials in the system design, the authors can make the system more efficient. In this view, reliability-based design optimization is a good way to come up with a proper design and development by combining other engineering techniques.

3.2. Gear teeth bending strength criterion

The first gear analysis was carried out by Wilfred Lewis et al. in 1892. The authors have created the so-called Lewis' equation. It has been acknowledged as the bending stress analysis of gear teeth[6]. Generally, the two primary causes for failures of the gears are tooth breakage and surface wear. Regarding the tooth breakage, excessive bending stress should be calculated to check strength of the tooth before manufacturing. The Lewis bending stress can be calculated by multiplying the maximum bending stress and a dimensionless Lewis form factor. In calculating the maximum bending stress, the torque due to power transmission, tangential load, and pitch line velocity should be calculated first. An advanced methodology, such as the AGMA bending stress, has been suggested to calculate the strength of gear teeth. This methodology was used to determine design variables in the gear teeth but can also be used as a constraint equation in optimization problems by introducing uncertainty to the design variables.

The authors used the AGMA bending stress methodology and equation to compare failure strength. Equations (22) and (23) are the gear teeth bending stress and the endurance limit. σ is the bending stress of a gear tooth, F_t is the gear mesh contact force, P is the tooth size, b is the tooth width, J is the gear geometry factor, K_v is the velocity or dynamic factor, K_o is the overload factor, K_m is a mounting factor, S_n is the bending fatigue strength, S'_n is the standard R.R. Moore endurance limit, C_L is the load factor, C_G is the gradient factor, C_S is a surface factor, k_r is the reliability factor, k_t is the temperature factor, and k_{ms} is the mean stress factor.

$$\sigma = \frac{F_t P}{b J} K_v K_o K_m, \quad (22)$$

$$S_n = S'_n C_L C_G C_S k_r k_t k_{ms}. \quad (23)$$

To satisfy the safety standards, bending stress should be lower than the endurance limit. In these equations, the variables except for the contact force F_t are known according to design of the gear. Our task is to find the contact force when the gear teeth bending stress is equal to the endurance limit (Equations (24),(25)). This contact force can be defined as the maximum gear mesh contact force $F_{t,max}$. Every gear mesh contact force should be lower than the maximum standards to avoid failure. The authors wrote a MATLAB code which calculates maximum gear contact force from gear information, performs numerical analysis including gear mesh contact force, and shows probability by comparing the gear mesh contact force with maximum standards.

$$\sigma_{max} - S_n \leq 0, \quad (24)$$

$$F_{t,max} \leq \frac{b J}{P K_v K_o K_m} S'_n C_L C_G C_S k_r k_t k_{ms}. \quad (25)$$

4. Results and discussion

4.1. Normal distribution curve of gear contact ratio

In reliability-based design optimization, uncertainty should be finally included to compare probability of each gear stage. In this research, the authors assumed that the contact ratio is treated as an uncertainty caused by manufacturing error. Fig. 3 shows a distribution of ring and planet gear contact ratio. Most of the values are concentrated around the mean value of the original contact ratio. One can express the probability of uncertainty by the probability of variables. Equation (26) shows the probability of variables.

$$x_i = \mu_i + \delta_i. \quad (26)$$

μ_i is the mean value of the variables, and the δ_i is the uncertainty of the variables. In mechanical manufacturing, errors follow a normal distribution. The normal

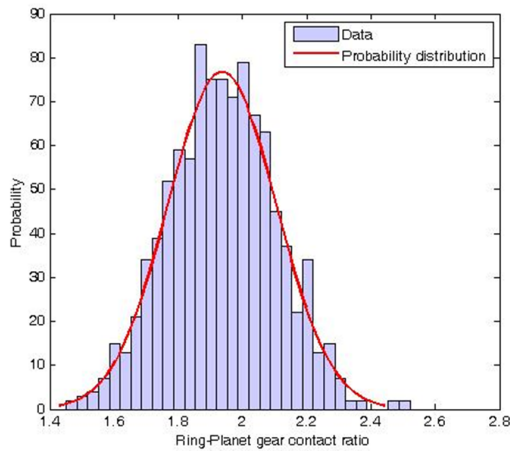


Fig. 3. Ring-planet gear contact ratio distribution in case of low uncertainty

distribution can be defined by the mean value and the standard deviation. Generally, the mean value is a basic dimension, and the standard deviation can be defined by equation (27).

$$\sigma_{x_i}^2 = T_{x_i}^2 / 9. \tag{27}$$

σ_{x_i} is the standard deviation of the gear mesh contact ratio and the T_{x_i} is the manufacturing error. Distributions are different when standard deviations differ. One can match standard deviation to manufacturing error. To guarantee objectivity, the authors simulated 3 cases which represent high, medium, and low uncertainties. It was shown that a large scale of allowance creates high uncertainty and high standard deviation. Fig. 4 shows the distribution of ring-planet gear contact ratio in high allowance cases. There can be seen a large range of variables and a wider distribution of probability compared to Fig. 3.

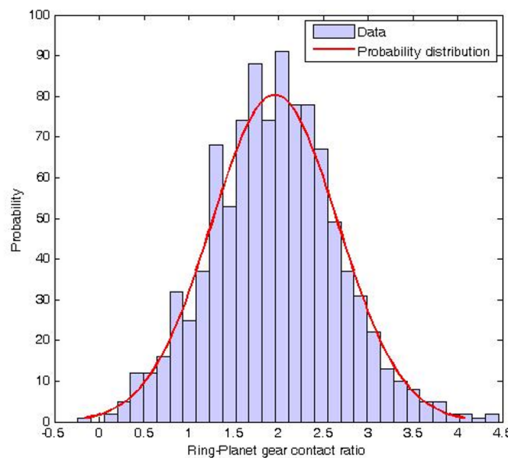


Fig. 4. Ring-planet gear contact ratio distribution in case of high uncertainty

4.2. Optimized number of gear teeth

In this section, the authors obtained an optimized gear teeth by applying MATLAB. Fig. 5 shows the MATLAB algorithm. To get reliable results, the authors simulated 1,000 calculations per design variable case. Additional considered cases represent high, medium, and low uncertainty, because gear mesh contact forces are significantly different for different contact ratios. By comparing the whole sets of data representing probability and reliability according the uncertainty, the algorithm have finally provided the best set of the optimized gear teeth. Table 2 shows the number of gear teeth optimized according to uncertainty. As it can be seen, all reliabilities are good when manufacturing error is low, and there are many cases in which gear teeth satisfy safety standards perfectly. But MATLAB code always follows a small number of gear teeth automatically. As referred, compliance should be minimized when constraint conditions are satisfied in reliability-based design optimization. This is the basic rule of optimization. The other fact is that reliability decreases and the number of gear teeth is generally greater when uncertainty is high. From this fact it follows that a greater number of gear teeth can improve reliability. With a bigger number of gear teeth, dynamic characteristics of rotation are

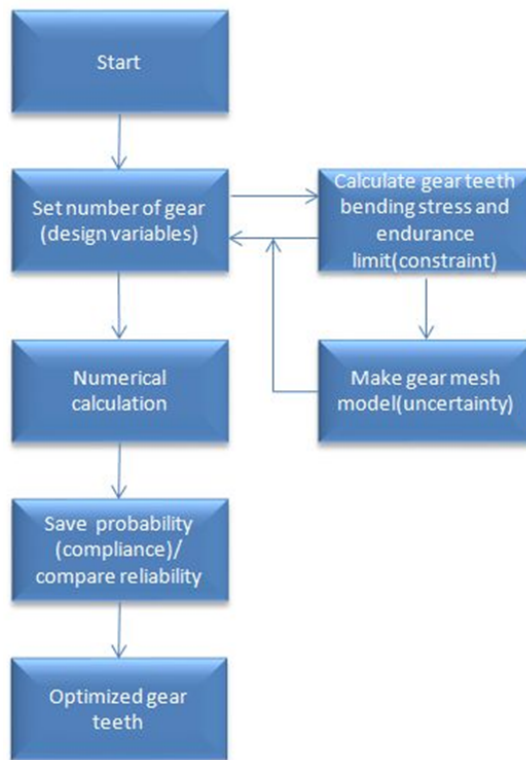


Fig. 5. Reliability based design optimization MATLAB algorithm

smoother and the gear mesh contact force is lower. It is the reason why the design of gear assures a proper backlash. In a gear system with a small number of teeth, there appears irregular vibration caused by the misalignment of gear. We called it the improper backlash. Reversely, the gear teeth will be regular if the number of gear teeth is bigger. However, the cost of manufacturing will be greater.

Table 2. Reliability in case of gear teeth uncertainty

	High uncertainty ($\sigma_{x,i} = 0.5$)	Medium uncertainty ($\sigma_{x,i} = 0.1$)	Low uncertainty ($\sigma_{x,i} = 0.01$)
Ring gear teeth	64	55	45
Sun gear teeth	16	14	12
Planet gear teeth	24	21	17
Gear 1 teeth	51	51	64
Gear 2-1 teeth	17	17	21
Gear 2-2 teeth	39	40	36
Gear 3 teeth	17	17	16
Reliability of sun-planet gear	83.2%	100%	100%
Reliability of ring-planet gear	84.0%	100%	100%
Reliability of gear 1-gear 2	81.9%	97.2%	100%
Reliability of gear 2-gear 3	82.1%	99.6%	100%

The graphs in Fig. 6 show an example of gear 2-gear 3 contact ratio and force distribution for a sample of 100 gears, whose characteristic is that the allowance is small. So, the authors inputted a well-designed gear contact ratio. As expected, the obtained contact force distribution corresponded to the gear contact ratio distribution. Due to the definition of gear contact force, its value was not negative. If an improper contact ratio is used, the gear contact force will increase. It is the reason why there are no negative values of gear force. Taking into account this fact, the authors found it necessary to consider the uncertainty of a system which makes an irregular output. Especially, the optimized solution never satisfies safety standards. Conversely, a solution that isn't optimized better satisfies safety and needs less maintenance expenditure compared to an optimized solution. To ensure a better accuracy, the authors ought to accumulate lots of data. If there were more samples in this example, a smoother normal distribution pattern would be obtained. The obtained reliability would satisfy a specific safe region related to this distribution.

According to these facts, the optimized gear teeth were designed so as to acquire high reliability in all cases. The number of teeth in the ring, sun, planet, gear 1, gear 2_1, gear 2_2, and gear 3 are 55, 14, 21, 51, 17, 40, and 17 when the standard deviation is 0.1, and the distribution satisfies reliability greater than 95%.

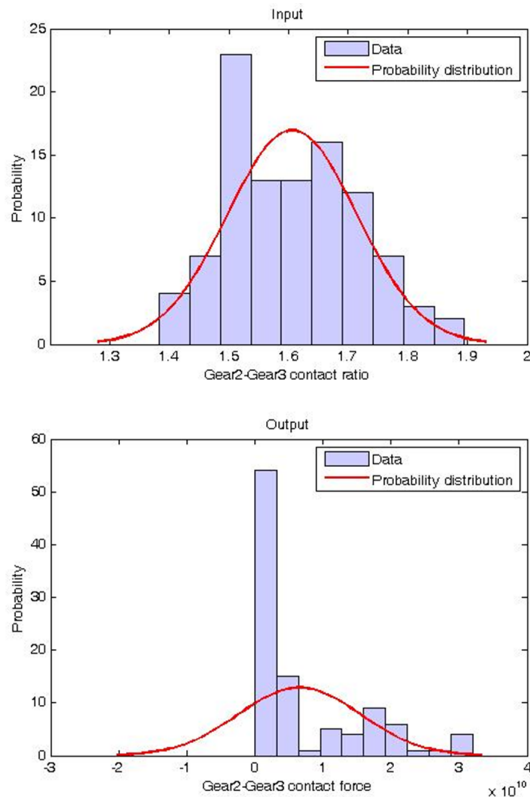


Fig. 6. Gear 2–gear 3 contact ratio, force distribution

5. Conclusions

In this research, the optimized gear teeth in the drive train system were developed by using the basic theorem of gear failure and reliability-based design optimization. Especially, the gear teeth contact ratios were the design variables with the uncertainty caused by the failure risk. Taking the uncertainty into account, the authors conducted the reliability-based design optimization determining the maximum gear contact force, carrying out drive train simulation, and comparing the obtained values to standards to find out the optimized number of gear teeth. For the optimization, the authors simulated the torsional drive train system with application of rotational coordinates. The authors established a static stress analysis model which gave information about endurance limit and bending strength. The equations of motion including the gear mesh models and kinematical relations in the drive train system were acquired based on a gear mesh stiffness model employing the Fourier series, the Lagrange equations and constraint equations. The numerical analysis was then carried out. Based on the results, such as the gear mesh contact force, the authors calculated the probabilities of failure, associated each

probability with the gear teeth, and determined reasonable and economic design of gear teeth.

Before applying the optimized gear teeth in the real system, the new design should be comprehensively checked, simulated, and thoroughly experimented to secure safety. To secure the reliability of the design, the drive train model including gear, shaft, and other components will be subjected to optimization based on flexible multi-body dynamics. Experimental works on dynamic characteristic of the drive train that utilizes the optimized gear teeth will be considered in the future.

Acknowledgements

This research is the result of financial support from “Yuhan University Research financial Support” and Software support from “Pohang of Metal Industry Advancement-Steel Pipe Center.”

References

- [1] S. Wang, T. Moan, and Z. Jiang. Influence of variability and uncertainty of wind and waves on fatigue damage of a floating wind turbine drivetrain. *Renewable Energy*, 181:870–897, 2022. doi: [10.1016/j.renene.2021.09.090](https://doi.org/10.1016/j.renene.2021.09.090).
- [2] Z. Yu, C. Zhu, J. Tan, C. Song, and Y. Wang. Fully-coupled and decoupled analysis comparisons of dynamic characteristics of floating offshore wind turbine drivetrain. *Ocean Engineering*, 247:110639, 2022. doi: [10.1016/j.oceaneng.2022.110639](https://doi.org/10.1016/j.oceaneng.2022.110639).
- [3] F.K. Moghadam and A.R. Nejad. Online condition monitoring of floating wind turbines drivetrain by means of digital twin. *Mechanical Systems and Signal Processing*, 162:108087, 2022. doi: [10.1016/j.ymssp.2021.108087](https://doi.org/10.1016/j.ymssp.2021.108087).
- [4] W. Shi, C.W. Kim, C.W. Chung, and H.C. Park. Dynamic modeling and analysis of a wind turbine drivetrain using the torsional dynamic model. *International Journal of Precision Engineering and Manufacturing*, 14(1):153–159, 2013. doi: [10.1007/s12541-013-0021-2](https://doi.org/10.1007/s12541-013-0021-2).
- [5] M. Todorov and G. Vukov. Parametric torsional vibrations of a drive train in horizontal axis wind turbine. In *Proceeding of the 1st Conference Franco-Syrian about Renewable Energy*, pages 1–17, Damas, 24-28 October, 2010.
- [6] R.C. Juvinall and K.M. Marshek. *Fundamentals of Machine Component Design*. John Wiley & Sons, 2020.
- [7] Q. Zhang, J. Kang, W. Dong, and S. Lyu. A study on tooth modification and radiation noise of a manual transaxle. *International Journal of Precision Engineering and Manufacturing*, 13(6):1013–1020, 2012. doi: [10.1007/s12541-012-0132-1](https://doi.org/10.1007/s12541-012-0132-1).
- [8] B. Shlecht, T. Shulze, and T. Rosenlocher. Simulation of heavy drive trains with multimegawatt transmission power in SimPACK. In: *SIMPACT Users Meeting*, Baden-Baden, Germany, 21-22 March, 2006.
- [9] M. Todorov and G. Vukov. Modal properties of drive train in horizontal axis wind turbine. *The Romanian Review Precision Mechanics, Optics & Mechatronics*, 40:267–275, 2011.
- [10] D. Lee, D.H. Hodges, and M.J. Patil. Multi-flexible-body dynamic analysis of horizontal axis wind turbines. *Wind Energy*, 5(4):281–300, 2002. doi: [10.1002/we.66](https://doi.org/10.1002/we.66).
- [11] F.L.J. Linden, P.H. Vazques, and S. Silva. Modelling and simulating the efficiency and elasticity of gearboxes, In *Proceeding of the 7th Modelica Conference*, pages 270–277, Como, 20-22 September, 2009.

- [12] J. Wang, D. Qin, and Y. Ding. Dynamic behavior of wind turbine by a mixed flexible-rigid multi-body model. *Journal of System Design and Dynamics*, 3(3):403–419, 2009. doi: [10.1299/jsdd.3.403](https://doi.org/10.1299/jsdd.3.403).
- [13] A.A. Shabana. *Computational Dynamics*. John Wiley & Sons. 2009.
- [14] A.K. Chopra. *Dynamics of Structures*. Pearson Education India. 2007.
- [15] Y. Park, H. Park, Z. Ma, J. You, J. and W. Shi. Multibody dynamic analysis of a wind turbine drivetrain in consideration of the shaft bending effect and a variable gear mesh including eccentricity and nacelle movement. *Frontiers in Energy Research*, 8:604414, 2021. doi: [10.3389/fenrg.2020.604414](https://doi.org/10.3389/fenrg.2020.604414).
- [16] S.R. Singiresu. *Mechanical Vibrations*. Addison Wesley. 1995.
- [17] R.R. Craig Jr and A.J. Kurdila. *Fundamentals of Structural Dynamics*. John Wiley & Sons. 2006.
- [18] K.J. Bathe. *Finite Element Procedures*. Klaus-Jurgen Bathe. 2006.
- [19] Y. Kim, C.W. Kim, S. Lee, and H. Park. Dynamic modeling and numerical analysis of a cold rolling mill. *International Journal of Precision Engineering and Manufacturing*, 14(3):407–413. 2013. doi: [10.1007/s12541-013-0056-4](https://doi.org/10.1007/s12541-013-0056-4).
- [20] S.J. Yoon and D.H. Choi. Reliability-based design optimization of slider air bearings. *KSME International Journal*, 18(10):1722–1729, 2004. doi: [10.1007/BF02984320](https://doi.org/10.1007/BF02984320).
- [21] H.H. Chun, S.J. Kwon, T. and Tak. Reliability-based design optimization of automotive suspension systems. *International Journal of Automotive Technology*, 8(6):713–722, 2007.
- [22] J. Fang, Y. Gao, G. Sun, and Q. Li. Multiobjective reliability-based optimization for design of a vehicledoor. *Finite Elements in Analysis and Design*, 67:13–21, 2013. doi: [10.1016/j.finel.2012.11.007](https://doi.org/10.1016/j.finel.2012.11.007).
- [23] Y.L. Young, J.W. Baker, and M.R. Motley. Reliability-based design and optimization of adaptive marine structures. *Composite Structures*, 92(2):244–253, 2010. doi: [10.1016/j.compstruct.2009.07.024](https://doi.org/10.1016/j.compstruct.2009.07.024).
- [24] G. Liu, H. Liu, C. Zhu, T. Mao, and G. Hu. Design optimization of a wind turbine gear transmission based on fatigue reliability sensitivity. *Frontiers of Mechanical Engineering*, 16(1):61–79, 2021. doi: [10.1007/s11465-020-0611-5](https://doi.org/10.1007/s11465-020-0611-5).
- [25] H. Li, H. Cho, H. Sugiyama, K.K. Choi, and N.J. Gaul. Reliability-based design optimization of wind turbine drivetrain with integrated multibody gear dynamics simulation considering wind load uncertainty. *Structural and Multidisciplinary Optimization*, 56(1):183–201, 2017. doi: [10.1007/s00158-017-1693-5](https://doi.org/10.1007/s00158-017-1693-5).
- [26] C. Luo, B. Keshtegar, S.P. Zhu, O. Taylan, and X.P. Niu. Hybrid enhanced Monte Carlo simulation coupled with advanced machine learning approach for accurate and efficient structural reliability analysis. *Computer Methods in Applied Mechanics and Engineering*, 388:114218. doi: [10.1016/j.cma.2021.114218](https://doi.org/10.1016/j.cma.2021.114218).